

Global coverage path planner in 2.5 dimensions for nonholonomic vehicles

Erik Arvidsson, Magnus Karlberg, Håkan Lideskog & Torbjörn Lindbäck

To cite this article: Erik Arvidsson, Magnus Karlberg, Håkan Lideskog & Torbjörn Lindbäck (17 Mar 2025): Global coverage path planner in 2.5 dimensions for nonholonomic vehicles, International Journal of Forest Engineering, DOI: [10.1080/14942119.2025.2469201](https://doi.org/10.1080/14942119.2025.2469201)

To link to this article: <https://doi.org/10.1080/14942119.2025.2469201>



© 2025 The Author(s). Published with
license by Taylor & Francis Group, LLC.



Published online: 17 Mar 2025.



Submit your article to this journal



View related articles



View Crossmark data

Global coverage path planner in 2.5 dimensions for nonholonomic vehicles

Erik Arvidsson , Magnus Karlberg , Håkan Lideskog , and Torbjörn Lindbäck 

Department of Engineering Sciences and Mathematics, LTU, Luleå, Sweden

ABSTRACT

This study presents a metaheuristic approach to coverage path planning for ground-based forest operations, focusing on minimizing path lengths for forest vehicles while considering terrain characteristics and vehicle parameters. Forest vehicles can usually tolerate higher pitch than roll angles, which makes them vulnerable to rollover. To mitigate that, this method utilizes a genetic algorithm to optimize the sequence of nodes, which are scattered over the site with equal spacing. The coverage path planner then calculates the Dubins path distance between every node in the fitness function, together with penalties for exceeding pitch, roll and soil moisture constraints for the vehicle. This ensures that the path planner tries to make the most traversable path as possible, while trying to minimize the driving distance. Two synthetic test sites resembling primitive challenging terrains, and one real site were utilized to theoretically evaluate the proposed method. The results show that aligning the node patterns with the critical slope headings, instead of having a straight pattern, had little effect on the path length. However, square grids can yield shorter paths across multiple runs, while triangular grids ensure consistent results in single runs. A two-hectare site took 43 minutes to calculate on average. This suggests that further development of the path planner could lead to significant improvements, enabling the management of sites larger than a few hundred nodes. However, the calculation time is justified for the reduced path length during deployment. The study presents a methodology that supports manual operators and establishes foundations for full autonomy.

ARTICLE HISTORY

Received 1 July 2024

Accepted 20 January 2025

KEYWORDS

Unmanned ground vehicle UGV; genetic algorithm GA; coverage path planning CPP; precision forestry; autonomous forest vehicle

Introduction

In Fennoscandia, the most common forestry method treats the forest in delimited sections, managing each stand consistently throughout its entire generation, which is called even-aged management (Savilaakso et al. 2021). The median area of harvested forest stands in Sweden was 2.2 hectares in 2022 (Swedish Forest Agency 2022b), and it is mandatory to replant the forest within three years after harvest according to the Swedish Forestry Act (Swedish Forest Agency 2022c). This is typically done by first mechanically preparing the site with a disc trencher or a moulder to reduce seedling mortality and increase growth (Örlander et al. 1990). After site preparation, manual planting is conducted in the prepared soil. Despite the benefits of site preparation, the action leaves a footprint in terms of soil disturbances. According to Sikström et al. (2020), the common techniques: mounding disturbs 37% of the total soil surface, while disc trenching disturbs 52%.

To mitigate this problem, Hansson et al. (2024) conducted autonomous site preparation and planting in a 30 cm spot diameter, with the aim of improving energy efficiency and minimizing soil disturbance. In simulation, the soil disturbance was below 3%. Although this proof-of-concept study did not provide detailed results in energy usage, it emphasized potential benefits such as reduced soil disturbances and the potential to decrease the size of forest vehicles.

In addition to site preparation, another significant factor contributing to soil disturbances in a forest is driving in too steep terrain and driving on soils with a high soil water content,

due to their higher risk of soil compaction (Jourgholami et al. 2022). Driving in too wet soil can lead to immobilization of the forest vehicle. Common cut-to-length forest machines such as forwarders can tolerate a higher pitch (tilt in driving direction) than roll angle (tilt in sideways direction) due to their longer wheelbase, while traversing a hill. This makes the forest machines vulnerable to rollover while driving in a side slope.

Since the mid-1970s, the amount of forest labor in Sweden has been reduced by half (Lund 2016). Simultaneously, the amount of felling has increased approximately 50%, where the largest productivity increase occurring in the late 1990s (Swedish Forest Agency 2022a). Currently, there has not been as significant progress and productivity has stagnated since the beginning of 2000. Despite the increasing automation over time, there remains further potential for reducing fuel consumption in forestry. This can either be done by planning better routes, using lighter vehicles, or changing methods on operations such as site preparation (Hansson et al. 2024).

Many forest vehicles, such as forwarders, are nonholonomic, meaning their movement is restricted by kinematic constraints. Due to their turning radii, forwarders can only move forward, backward with various turning angles. Unlike holonomic vehicles, which can move sideways directly, forwarders combine forward or backward motion with turning to achieve lateral movement.

As modern forest vehicles have experienced size and load capacity increases (Nordfjell and Emil Öhman 2019), their productivity has increased. However, this has come at the expense

of greater soil disturbance. One potential solution is to adopt autonomous forest vehicles that are both lighter and smaller than the current machines, reducing soil impacts while maintaining operating productivity. These systems could potentially operate twice as many productive hours annually compared to current forest machines, at half the hourly productivity rate, thereby reducing damage while maintaining overall productivity levels (Ringdahl 2011).

By reducing the formfactor of vehicles, the transition to full autonomy needs to occur directly to sustain productivity. Focusing on coverage path planning instead, an adoption can be done over time. The initial implementation can begin by serving as a support tool for manual operators. As technology advances and matures, it can then be gradually integrated into fully autonomous vehicles.

Coverage path planning is a technique that is applied for coverage-based applications such as robotic vacuum cleaners (Yasutomi et al. 1988), various Unmanned Aerial Vehicle operations (Cabreira et al. 2019), as well as sowing and tilling operations in agriculture (Han et al. 2022). Research on coverage path planning in agriculture has been explored in both 2D and 3D approaches. In 2D planning, a common method is boustrophedon cell decomposition, where fields are divided into simpler cells and covered using back-and-forth motions for complete coverage (Choset 2000). In 3D approaches, researchers have been focusing on optimizing driving direction of field-work tracks and their sequence to reduce energy consumption (Hameed 2014; Dogru and Marques 2015a), as well as minimizing overlapping errors that can occur during projection from an elevation surface to 2D (Hameed et al. 2016). An alternative approach involves utilizing seed curves instead of straight lines to follow the terrain of the field (Jin 2009; Bostelmann-Arp et al. 2023). Commonly, these articles share a focus on reducing energy consumption. However, they are allowed to drive in every direction within the field, as most agricultural fields are established on terrain with good traversability. In a forest terrain, aggressive slopes, wet areas, and other non-traversable areas need to be considered.

For uneven terrain, Qiu et al. (2024) created a coverage path planner suitable for Unmanned Ground Vehicles (UGV), which used terrain traversability analysis to avoid dangerous zones. They solved it by segmenting the Digital Elevation Model (DEM) into a traversability map. Then, different seed paths were grown on the test sites until the entire area was populated. Thereafter, a genetic algorithm optimized the sequence of seed paths. This study addressed the roll and pitch angles of the vehicle to prevent it from attempting non-traversable paths. Additionally, a turning cost was applied, although a specific turning radius was not considered. This approach may present challenges for vehicles with a larger turning radii.

Wu et al. (2019) created a coverage path planner for UGV's, where a heuristic algorithm was applied to create geodesic Fermat spirals based on the 3D surface. With this approach, their goal was to follow the contour lines of the elevation to reduce energy consumption. However, this work did not consider the turning radius of the robot, nor the traversability constraints if a slope became too steep for the vehicle in either the roll or pitch direction, which is important in forest vehicle path planning.

Hansson et al. (2024) developed a coverage path planner adapted for forest regeneration, prioritizing minimized driving time while accounting for penalties associated with sharp turns, steep slopes, and seed capacity limitations. The planner also excludes areas with high soil moisture. To achieve this, the field was divided into hexagonal cells, with each cell evaluated for slope magnitude and heading. Cells were then grouped based on adjacency to determine common driving line headings. The length of driving lines was adjusted for optimal alignment with neighboring lines. Lastly, a Traveling Salesman Problem (TSP) was solved to establish an efficient sequence for the driving lines, considering machine specifications such as working width, total time, and cost, including turning penalties. However, the planner did not calculate specific turning radii, potentially resulting in paths unsuitable for vehicles with large turning radii, leading to additional detours.

Although some research has been conducted on path planning in offroad areas, there is still a lack of knowledge regarding vehicle and terrain specific constraints in forestry, including wet zones, terrain slope and vehicles with large turning radii, e.g. forest vehicles. These important factors will be addressed in this paper.

Aim, objective and scope

The overall aim of this study is to facilitate efficient driving of utility vehicles in terrain for coverage-based tasks. The objective is to develop a method for a Global Coverage Path Planner (GCPP) that produces short complete routes for nonholonomic vehicles in challenging terrain, by only driving the vehicle forward. The path should also consider soil moisture and allow various vehicle parameters like turning radius, safe roll and pitch angles. To ensure vehicle safety, any solutions that exceed these constraints must be avoided.

Examples of application areas for this work are forest scarification, planting robots, forest fertilization, ground-based surveying, or other ground-based terrain operations that need to cover an area. Smaller obstacles such as boulders and shelterwood/seed trees are assumed to be managed by the local path planner.

Materials and methods

The GCPP in this article operates according to the flowchart illustrated in Figure 1. It begins by receiving several inputs: a Shape-file delineating the site boundary, a DEM for slope analysis, a soil moisture map to avoid wet areas, and vehicle parameters such as turning radius, working width, and maximum roll and pitch angles to consider vehicle kinematics. These inputs are used to generate nodes that all need to be visited.

The sequence in which nodes are visited is determined by a Genetic Algorithm (GA). The GA iteratively seeks to find the shortest path while ensuring the vehicle avoids wet areas, avoids crossing neighboring site boundaries, and adheres to vehicle kinematics constraints. The GA terminates its calculations either upon reaching a maximum number of iterations or if the result from the fitness function converges for a set number of iterations.

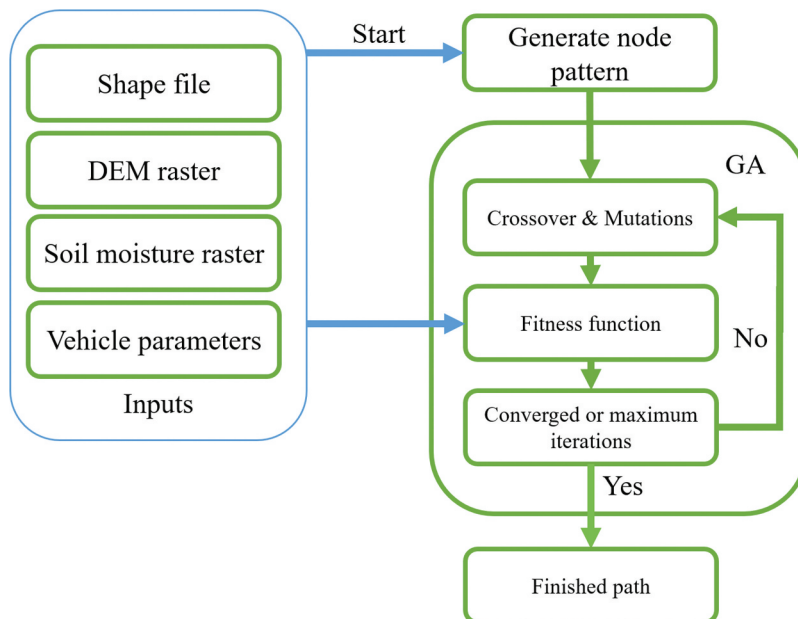


Figure 1. The flowchart of how the path planner was calculated.

Certain operations, such as calculating path length and coverage, are conducted in 2D to reduce complexity and computational time. Meanwhile, vehicle kinematics considers slope magnitude and aspect discretely. This approach is the reason for naming this work “Global coverage path planner in 2.5 dimensions for nonholonomic vehicles.”

Map

The goal of the TSP is to find the shortest possible route that visits a given set of nodes once. In other words, it seeks to determine the most efficient way for a traveling salesman to visit all the nodes in their territory, minimizing the total distance traveled. The challenge of the TSP lies in its combinatorial nature, as the number of possible routes grows exponentially with the number of nodes, making it computationally demanding to find the optimal solution for large instances. Given the computational demanding nature of the TSP, minimizing the number of nodes to be processed can significantly improve computational efficiency. Therefore, a grid of nodes is distributed across the site that may still fulfill an area coverage demand if all nodes are visited. The TSP will

then calculate the order in which each node will be visited to create the shortest path.

In this study, two distinct grid discretization techniques, a square grid, and an equilateral triangular grid, are evaluated. Both implemented in a two-dimensional space and then projected vertically onto the DEM.

The discretization process involves arranging the nodes in a triangular or a square pattern. The triangular pattern setup allows each node to have six equidistant neighboring nodes, while the square grid only permits four neighboring nodes. Consequently, the triangular grid offers a larger number of options for node visitation, which was assumed to be advantageous for articulated vehicles considering their turning radius. The scattered nodes are only placed in areas where soil moisture and elevation gradients match user-defined constraints. Outside of the constraints, nodes are not placed which is displayed in [Figure 2](#). Consideration is not given to mitigate potential difficulties that can occur by placing nodes near the site border or alongside areas exceeding user constraints. The spacing between scatter nodes is set to match the vehicles working width to minimize overlap. However, minimizing overlap in areas with sharp turns can result in gaps ([Jin and Tang 2011](#)).

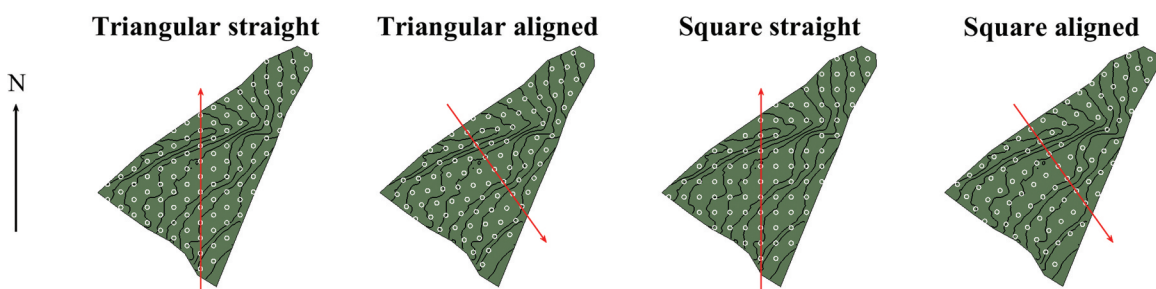


Figure 2. Test site with different discretization techniques, with nodes presented with white rings. The grids are aligned with the red arrows, which for the mean critical slope aspect is headed towards southeast, and the straight towards north. The black lines represent elevation contour lines, spaced one meter apart. The avoidance of nodes in the middle of the site is caused by steep slopes, while the avoidance in the lower right area is caused by high soil moisture.

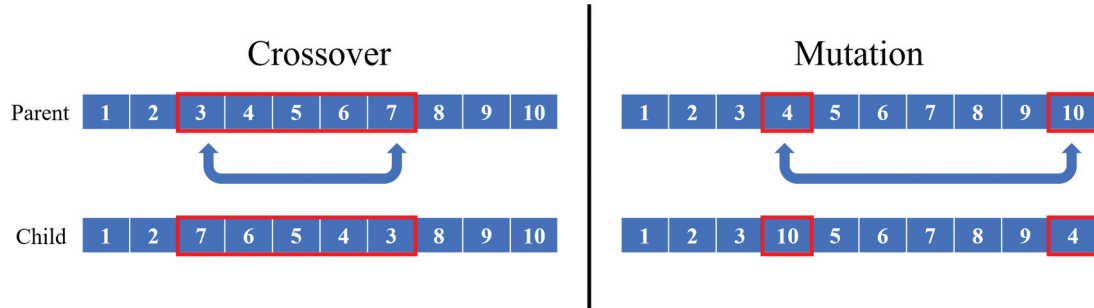


Figure 3. Crossover to the left involves flipping a segment between two arbitrary nodes of the permutation, while mutation to the right only changes the position of two arbitrary nodes.

Experimentation also includes rotating the node grids around the centroid of the test site, as displayed in Figure 2. The hypothesis was that aligning the grid with the mean slope aspect of the DEM within specified gradient thresholds, can assist the path planner in critical slope areas. The straight pattern, which always faces north, serves as a reference in the tests. Totally there are four different grid patterns per test site compared in the study, a triangular straight, a triangular aligned, a square straight and a square aligned, all represented in Figure 2.

Genetic algorithm

Now that we have determined the placement of the nodes, we aim to identify the optimal sequence for visiting all nodes. To determine the best sequence, we apply a GA.

The GA is based on the biological process of natural selection. The best candidates of a generation get to mate with the other best candidates to hopefully create offspring that are even better than their parents. To determine candidates, a fitness function is used to quantify their performance (Man et al. 1996). In the TSP, the fitness function is often determined to find the shortest path while visiting all nodes.

The application of the GA aims to optimize the sequencing of nodes, with a strategy to determine a discrete path characterized by minimal Dubins path (see the Dubbins path section below) distance while preventing rollovers, avoiding wet areas, and ensuring no crossing of site borders.

The GA in this study begins by generating multiple random sequences based on all the nodes in the grid, with the number of sequences matching the population size. After that, the GA creates new permutations, as many as the population size, and then the GA evaluates whether the fitness value is smaller than in the previous generation. If the fitness value is smaller, the permutation is kept, and if it is higher, it is discarded. The smallest distance from each batch is extracted, and these batches are referred to as generations, to be used in breeding for future iterations. The permutations with the smallest distance are called elite and are kept for the next generation to have a mix in the genetic pool.

There are mainly two different mechanisms that can generate better solutions: crossover permutations and mutations. Crossover mimics mating, where a chromosome from two parents is mixed to create a new permutation. Other crossover functions flip an arbitrary section of a single node

```

Initialize population with random individuals
Evaluate Fitness of each individual
generation = 0
stall = 0
while (generation < Max Generations) or (stall < Max Stall Generations) do
    Select parents from population
    Perform crossover to create offspring
    Perform mutation on offspring
    Calculate Fitness(generation), described in section 2.3.1
    Select survivors for next generation
    if min(Fitness(generation)) == min(Fitness(generation - 1)) then
        stall ← stall + 1
    else
        stall = 0
    end if
    generation ← generation + 1
end while
return min(Fitness(generation))

```

sequence, which is the crossover function used in this work, which can be seen in the left side of Figure 3. The mutation function used in this work switches place of two arbitrary nodes in the node sequence, which can be seen in the right side of Figure 3. Mutations are mainly used for escaping local optima, enabling the solver to advance toward the global optimum.

Since GA computes results for entire genes, they offer the advantage of accommodating complex fitness functions. This capability allows for the examination of multiple nodes within a sequence, which is shown in Algorithm 1, where the GA is described.

$$\delta_i = \frac{\text{atan}2(\text{node}_{y_{i+1}} - \text{node}_{y_i}, \text{node}_{x_{i+1}} - \text{node}_{x_i}) + \text{atan}2(\text{node}_{y_i} - \text{node}_{y_{i-1}}, \text{node}_{x_i} - \text{node}_{x_{i-1}})}{2} \quad (1)$$

Dubins path

Since common cut-to-length forest vehicles have articulated joints with relatively large turning radii, the turning radii cannot be neglected. In many TSP solvers, the Euclidean distances are used, which is the shortest path between two nodes without any turning radius constraint. The shortest path between two nodes with a specified turning radius is called a Dubins path (Dubins 1957) and is therefore a more suitable solution for this application than calculating the Euclidean distances. Dubins paths rely on either having a max steering angle to the left, driving straight or having a full steering angle to the right (Dubins 1957). To determine a Dubins path in 2D for each permutation, four inputs are needed: the x- and y-values of the nodes, the Dubins heading δ_i of each node and the turning radius of the vehicle. To determine δ_i through each node i , the average heading angle between the two vectors, built by the two nearby nodes $i-1$ and $i+1$ in the permutation, was calculated using Equation 1:

For the start and end node, the heading was set to the angle between the current and the next/previous node.

Fitness function and penalties

The fitness function that the GA is trying to minimize is P_{tot} , which is the sum of Dubins path length and penalties and is defined in Equation 2:

$$P_{tot} = P_{dist} + \sum P_{rollover} + \sum P_{moist} + \sum P_{neighbor} \quad (2)$$

where P_{dist} calculates the two-dimensional Dubins path between nodes in the specified order determined by the GA permutation. To ensure proximity between the start and end nodes, the first node of the permutation is appended again at the end. This arrangement facilitates computing the entire path as a closed loop, offering flexibility to cut the loop at desired nodes for determining the vehicles start and stop positions. It is important to note that this additional node is not included in further breeding processes; it is solely utilized to compute the fitness value.

The traversable angles for each point along the Dubins path are calculated by investigating roll and pitch angles along every second meter (the same distance as the DEM resolution) along the path from that permutation, which is described by Equations 3 and 4:

$$\alpha_{pitch}(x, y, \theta_{vehicle}) = \alpha_{slope}(x, y) \cdot |\cos(\theta_{vehicle} - \theta_{slope}(x, y))| \quad (3)$$

$$\alpha_{roll}(x, y, \theta_{vehicle}) = \alpha_{slope}(x, y) \cdot |\sin(\theta_{vehicle} - \theta_{slope}(x, y))| \quad (4)$$

where $\alpha_{pitch}(x, y, \theta_{vehicle})$ and $\alpha_{roll}(x, y, \theta_{vehicle})$ represent the pitch and roll angle of the vehicle, respectively, for the location of the vehicle.

$\alpha_{slope}(x, y)$ denotes the magnitude of the slope. $\theta_{slope}(x, y)$ signifies the aspect of the gradient for the cell, and $\theta_{vehicle}$ corresponds to the vehicle heading, which can be seen in Figure 4. Both angles have a heading of 0° when facing north and 90° when facing east.

If a point on the path is given outside the traversable angles ($\alpha_{pitch}(x, y, \theta_{vehicle}) > \alpha_{max\ pitch}$ or $\alpha_{roll}(x, y, \theta_{vehicle}) > \alpha_{max\ roll}$), a penalty of 100 meters is added to $P_{rollover}$ to prevent rollover. The moisture penalty is also calculated by following the Dubins path every second meter, but if the path is placed at a coordinate where the soil moisture is higher than the user constraint, then P_{moist} is set to 100 meters. Another penalty of 10,000 meters is added to $P_{neighbor}$ if the GA chooses a permutation where a Pythagorean line between two consecutive nodes crosses the border to the neighboring site. This is introduced to prevent the path planner from taking shortcuts on concave sites. The magnitude of the penalties is derived from empirical studies. When a penalty was set too low, the GA proposed solutions ignoring the constraints. In contrast, setting a penalty too high often trapped the GA in local minima. The reason why the penalty magnitude of $P_{neighbor}$ is larger than $P_{rollover}$ and P_{moist} is that $P_{neighbor}$ is assessed between every node, whereas the others are evaluated along the Dubins path, which includes more evaluation points. To calculate the fitness function for the GA, Algorithm 2 is used.

Test sites

In agriculture, different benchmark sites exist, e.g. Nilsson and Zhou (2020) who created 54 standard fields. The standardized fields are different shaped polygons that are in arbitrary

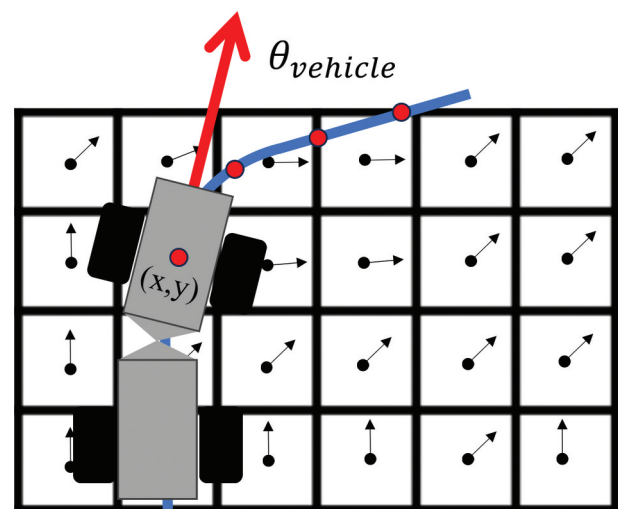


Figure 4. The black dots with arrows represent the digital elevation model-raster along with its corresponding aspect $\theta_{slope}(x, y)$. Each raster cell also contains slope magnitude $\alpha_{slope}(x, y)$ and $\text{Soil}_\text{moisture}(x, y)$ values. The vehicle follows the Dubins path shown in blue, and at every second meter (matching the DEM resolution), the values $\alpha_{pitch}(x, y, \theta_{vehicle})$ and $\alpha_{roll}(x, y, \theta_{vehicle})$ are calculated at the red dots. The heading $\theta_{vehicle}$ of the vehicle is shown by the red arrow and is tangent to the Dubins path. The top of the figure corresponds to North (y), and the right corresponds to East (x).

positions. But the model lacks DEM, which makes it less relevant as a benchmark in forestry operations since elevation is critical to consider in terrain path planning.

Consequently, two different synthetic test sites are created to determine the performance of the path planner, attempting to mimic the test sites of Dogru and Marques (2015a). The synthetic site size is modified to fit the mean harvest area in Swedish forestry, that is going to be replanted. The synthetic test sites are created by drawing a square of the 2D area of 2.0 ha. The elevation is then set to 1 m in the low section and 10 m in the high section. The transition is made with a 2D Gaussian filter with $\sigma = 10$, together with a grid size of the synthetic DEM of 2×2 m, resulting in a maximum slope of 10.47° . The $\text{Soil}_{\text{moisture}}$ is set to 50 units on the entire site on all the synthetic sites. The test sites are shown in Figure 5.

Test site 1 is a real test site. It has a 2D area of 2.0 ha and an elevation difference of 11.0 m. The test site is outside of Älvbyn, Sweden at WGS84 coordinate $65^\circ 40' 47''\text{N}$ $21^\circ 12' 34''\text{E}$.

As mentioned earlier during discretization, the aspect of the site can be used to align the grid. In Figure 6(a), the aspect at site 1 is shown, along with the critical aspects, which are displayed in Figure 6(b). The mean critical aspect, calculated from Figure 6(b), is 143° and corresponds to a southeast direction.

Parameters

The parameters for the GA were derived through empirical studies. The “Population Size” and “Elite Count” were initially

set to larger values and then gradually reduced to achieve similar results with shorter computation times. Setting the “Max Generations” parameter too low caused the algorithm to terminate prematurely, while a too high setting led to longer runtimes without finding better solutions. Observations indicated that crossover played a critical role in the early stages of the calculation, while mutation became more significant toward the end. The performance of certain parameter combinations can vary depending on the site and grid patterns, though. Some combinations may work well for one location but perform poorly for another. In this study, the set of parameters are:

- Population Size: 60
- Elite Count: 10
- Crossover: 70%
- Mutation: 20%
- Max Generations: 60 000
- Max Stall Generations: 10 000

These provided stable results throughout all sites and grid techniques and were therefore selected. The vehicle parameters describe the Research Vehicle Platform, which is Luleå University of Technology’s test vehicle for autonomous forest operations (Lideskog et al. 2015). The research vehicle weighs approximately ten metric tons and is equipped with a Cranab FC8 crane that has approximately 9 meters of reach (Hera et al. 2024; Hansson et al. 2024). Due to the size of the crane compared to the vehicle, it risks tipping while operating at full

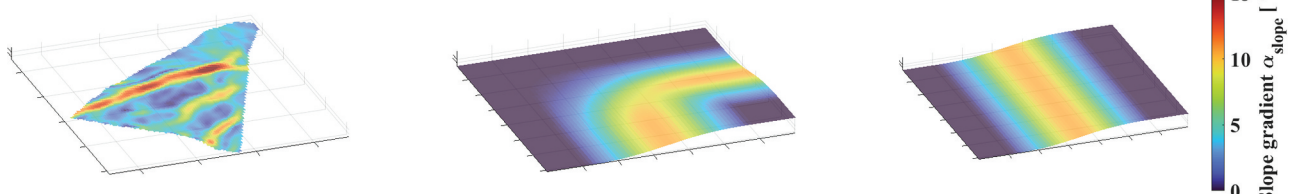


Figure 5. The real test site (left) is site 1. Site 2 (middle), and site 3 (right) are synthetically created. In this work, the maximum roll angle is set to 8° , and the maximum pitch angle is set to 15° . Thus, the vehicles heading is critical on these sites to prevent rollovers. Site 1 features areas marked in dark red that must be completely avoided. Due to higher tolerance in pitch than roll, sites 2 and 3 have areas that can only be traversed in one direction.

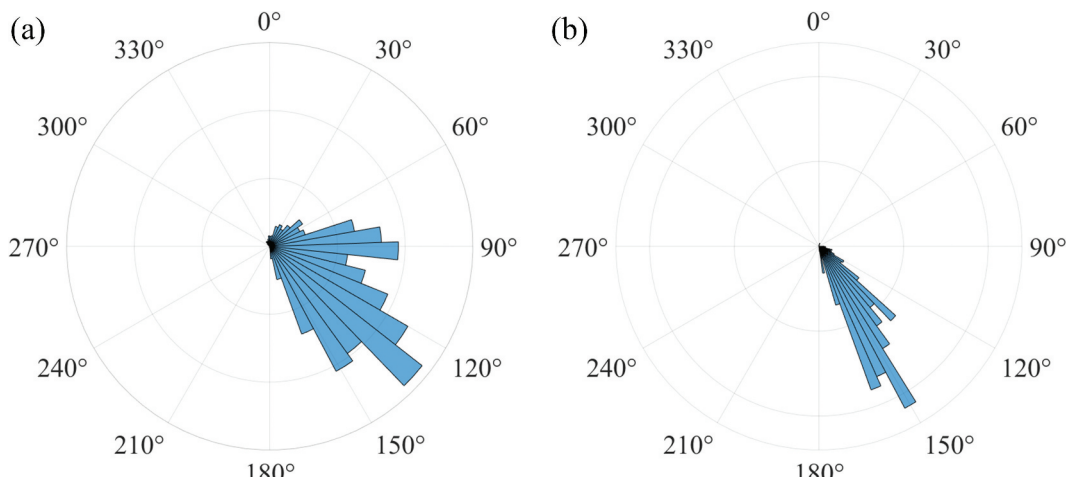


Figure 6. Slope aspect (θ_{slope}) for all DEM cells within site 1 is shown in Figure 6(a), and for DEM cells with a gradient (α_{slope}) between the critical angle span $\alpha_{\text{max roll}}$ and $\alpha_{\text{max pitch}}$ within the same site is shown in Figure 6(b). Additionally, Figure 6(b) enables determination of the mean aspect, which is used for aligning the node pattern.

reach. Therefore, a safe reach approximation of 7.5 meters is adopted, resulting in a circular working width of 15 meters. The parameters used in the study are the following:

- Turning radius: 4.6 m
- Working width: 15 m
- Max roll angle ($\alpha_{max\ roll}$): 8°
- Max pitch angle ($\alpha_{max\ pitch}$): 15°
- Max soil moisture ($Soil_{max\ moisture}$): 90

These values correspond to relatively small forestry vehicles, as typical cut-to-length vehicles can weigh more than twice as much (Nordfjell et al. 2010; Nordfjell and Emil Öhman 2019). A larger vehicle working width results in the need for shorter path distances. However, a larger working width typically requires larger equipment, leading to heavier vehicles. Furthermore, when using a crane-operated planting vehicle (Hansson et al. 2024), a wider working width also results in a lower driving velocity for the base vehicle.

The coordinates and map data within this study are primarily calculated within the SWEREF99 TM projection. The elevation data used in this study are provided from the Swedish mapping, cadastral and land registration authority “Lantmäteriet.” The DEM “GSD-Höjddata grid 2+,” has a spatial resolution of two meters and has the national transverse Mercator projection SWEREF 99 TM. The DEM has a vertical accuracy of 0.1 m and a spatial accuracy of 0.3 m (Lantmäteriet 2024). The soil moisture model used in this study was developed by the Swedish University of Agriculture (Lidberg 2019) and has a spatial resolution of two meters and is also presented in SWEREF 99 TM.

Calculations

The coverage of the test sites is calculated in 2D by creating a polygon formed from the union of circles with diameters equal to the vehicles working width, centered at points along the Dubins path. This polygon provides padding along the path. The intersection between the Dubins polygon and the test site polygon determines the area within the test site boundary covered by the vehicle. The coverage fraction is obtained by dividing the area of the vehicle coverage by the total area of the test site.

The calculations were performed on an Intel Core i9 10900K 3.7 GHz CPU, 32 GB of RAM, and a Nvidia GeForce RTX 3090 GPU. Notably, the GPU is minimally utilized, as the computational demands of the problem primarily relied on the CPU. The operating system used is Ubuntu 22.04.03 LTS. The software used is *MATLAB R2023b*, with the toolboxes *Mapping Toolbox* to handle all the map data, *Global Optimization Toolbox* for handling the GA solver and *Navigation Toolbox* for adopting the Dubins curves.

Since the GA relies on a random number generator to initialize the population and to select nodes for its crossovers and mutations, conducting multiple tests and statistically comparing the results gives a representative result. The tests were compared using a two-sided Mann–Whitney U-test (Mann and Whitney 1947), due to the limited sample size and the observation that the results did not appear to follow a Gaussian distribution. Each test site was calculated multiple times, with the number of runs per site adjusted to achieve a significance level below 1%, ensuring accurate comparisons between the different node

```

for node  $i$  in permutation do
    if line between current node  $i$  and  $i + 1$ , crosses site border then
         $P(i)_{neighbor} = 10\ 000\text{m}$ 
    end if
end for

 $P_{dist} = \text{Dubins path length sum}$ 

for point  $j$  on Dubins path, with same spacing as the DEM resolution do
    if  $(\alpha(j)_{roll} > \alpha_{max\ roll})$  or  $(\alpha(j)_{pitch} > \alpha_{max\ pitch})$  then
         $P(j)_{rollover} = 100\text{m}$ 
    end if
    if  $Soil(j)_{moisture} > Soil_{max\ moisture}$  then
         $P(j)_{moisture} = 100\text{m}$ 
    end if
end for

return  $P_{Tot} = P_{dist} + \sum P_{rollover} + \sum P_{moist} + \sum P_{neighbor}$ 

```

configurations. Hence, the required number of repetitions differs between test sites.

Results

Table 1 summarizes the results from the multiple runs conducted for each test site configuration. The study compares two grid patterns and evaluates two grid rotations. The first grid rotation aligns the nodes of the grid with the mean critical slope aspect, while the second involves no rotation. The table also shows the calculation times for various configurations in single-core mode. On average, it took 42.8 minutes to compute one run at one test site.

To ensure a fair comparison between the methods, var-

the extent of site coverage achieved by different solutions. The results, shown in **Table 2**, indicate that the aligned pattern exhibits a shorter path length [m] in four out of six site setups with statistical significance. The same trend is observed when comparing path length per coverage [m %⁻¹]. However, when examining path length per coverage per node [m %⁻¹node⁻¹], the aligned pattern is only superior in two out of six site setups with statistical significance. The aligned pattern performed best on site 3 for both the triangular and square grid, while the result varied on site 1 and 2.

Results from triangular and square grid are shown in **Table 3**. The square grid demonstrated shorter path lengths [m] in five out of six site setups, with a significance level below 1%. When

Table 1. Performance metrics comparing configurations, evaluating three test sites with different grid patterns and grid rotations. Note that the triangular grid pattern converges to the same result over all its runs, while the square grid pattern varies.

	Number of runs	Grid pattern	Grid rotation	Number of nodes	Median path length [m]	Min and Max path length [m]	Mean coverage [%]	Mean calculation time[min]
Site 1	26	Square	Aligned	86	1982	1535 2032	92.5	32
			Straight	85	1962	1540 2379	93.4	39
	29	Triangular	Aligned	94	1868	1868 1868	92.8	38
			Straight	101	2019	2019 2019	96.3	50
Site 2	29	Square	Aligned	89	1681	1595 1681	95.8	38
			Straight	100	1873	1684 1873	98.1	50
	14	Triangular	Aligned	102	1948	1948 1948	97.2	46
			Straight	104	1927	1927 1927	98.6	42
Site 3	29	Square	Aligned	100	1569	1569 1701	98.2	47
			Straight	100	1686	1620 1736	98.2	45
	14	Triangular	Aligned	104	1822	1822 1822	96.9	40
			Straight	104	1934	1934 1934	98.7	46

Table 2. Comparison between straight node pattern and node pattern aligned toward the mean critical slope heading. The method displayed in each cell of the table is the corresponding method with the lowest value, with a p-value of 0.01 or lower.

Site number	Node pattern	Site 1		Site 2		Site 3	
		Triangular	Square	Triangular	Square	Triangular	Square
Path length [m]		Aligned	Straight	Straight	Aligned	Aligned	Aligned
Path length per coverage [m/%]		Aligned	Straight	Straight	Aligned	Aligned	Aligned
Path length per coverage per node [m/(%*node)]		Straight	Straight	Straight	Straight	Aligned	Aligned

Table 3. Comparison between triangular and square node pattern. The method displayed in each cell of the table is the corresponding method with the lowest fitness value, with a p-value of 0.01 or lower.

Site number	Node pattern	Site 1		Site 2		Site 3	
		Straight	Aligned	Straight	Aligned	Straight	Aligned
Path length [m]		Square	Triangular	Square	Square	Square	Square
Path length per coverage [m/%]		Triangular	Triangular	Square	Square	Square	Square
Path length per coverage per node [m/(%*node)]		Triangular	Triangular	Triangular	Triangular	Square	Square

ious comparison parameters are established. This approach aims to address differences in the number of nodes across different test sites and grid patterns, as well as variations in

evaluating path length per coverage [m %⁻¹], the square grid had a lower mean value in four out of six site setups. However, for path length per coverage per node [m %⁻¹node⁻¹], the triangular

grid performed better than the square grid in four out of six setups. Although the square pattern achieved the best performance across all parameters on site 3, the outcomes varied for sites 1 and 2.

The comparisons were made based on running the calculations multiple times per configuration to evaluate the performance of the tool since it relies on a random number generator. The number of runs was iterated until it could demonstrate that all cells in [Tables 2 and 3](#) had a significance level lower than 1%. The number of runs per site is shown in [Table 1](#).

The shortest path of each site is presented in [Figures 7–9](#), where the surface is presented as the DEM, the surface color is the gradient magnitude, the white dots are the nodes that the

path needs to pass, and the light green lines comprise the path that the GA has calculated.

[Figure 7](#) also shows that the GCPP successfully avoids the areas where the gradient magnitude exceeds the vehicle constraints, ensuring vehicle safety.

Discussion

This study represents an advancement in enabling autonomous ground vehicles to operate effectively in rugged terrains, characterized by constraining soil moisture, turning radii, pitch and roll allowances. By developing a GCPP tailored for nonholonomic vehicles in 2.5 dimensions, this work not only supports autonomous navigation but can also aid manual operators in

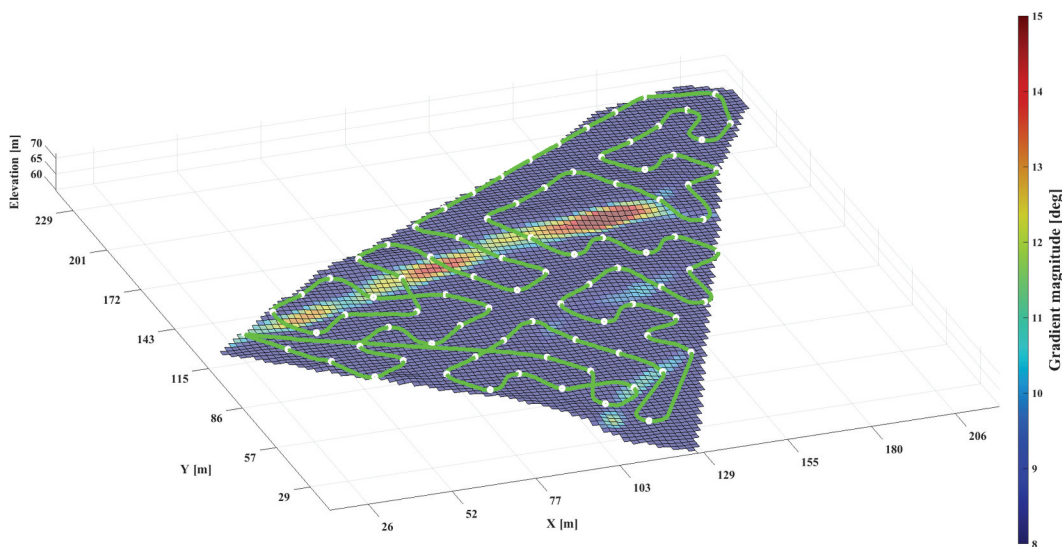


Figure 7. Shortest path length of all runs and configurations of site 1, which has a square and aligned node pattern. The total path length is 1 535m. The path avoids a cliff located in the center of the field, where nodes were not inserted by the program. The GA also avoided traversing the steep section of the terrain exceeding 15°, and only drove along the critical slope aspect in each DEM cell.

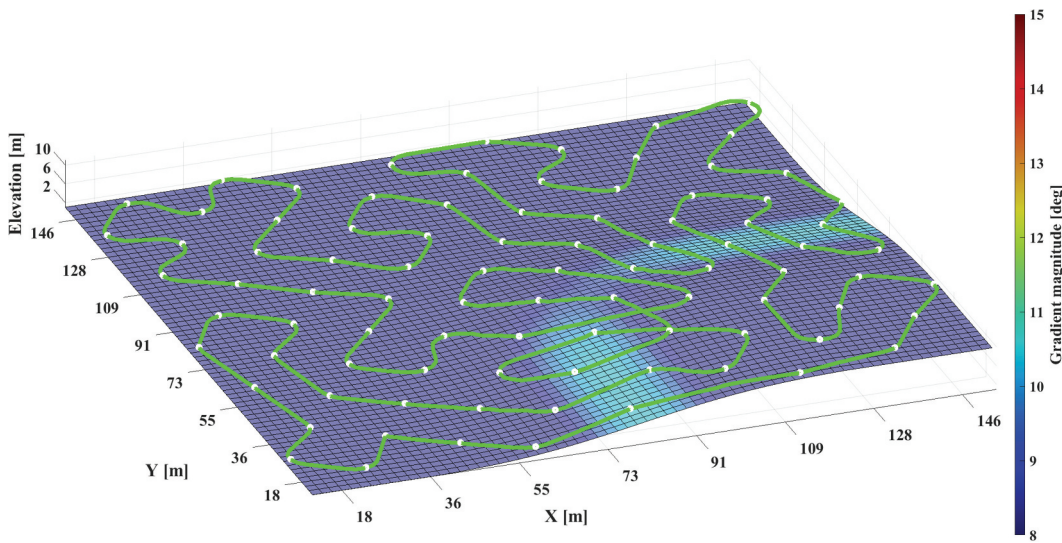


Figure 8. Shortest path length of all runs and configurations of site 2, which has a square and aligned node pattern. The total length of the path is 1 595m. The results show a path without penalties, leading to a path that only traverses the slopes in the aspect direction.

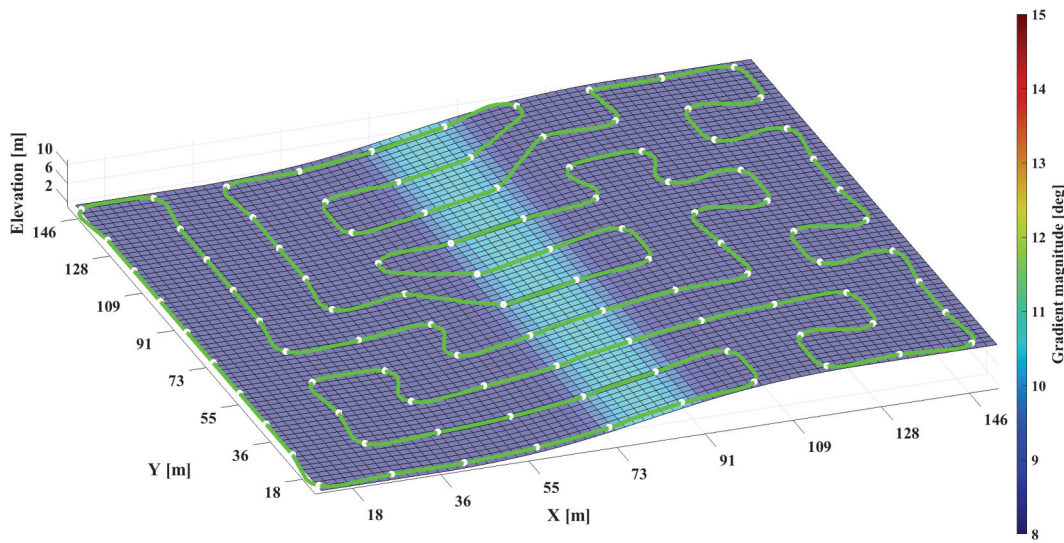


Figure 9. Shortest path length of all runs and configurations on site 3, which has a square and aligned node pattern. The total length of the path is 1 569m. Like the previous sites, the coverage path planner computed a path without penalties, only traverses the critical slope along its aspect.

following a safe path and assessing the feasibility of vehicle maneuvers in specific areas. The transition difficulties from manual operation to full autonomy are thus reduced, enabling a smoother switch.

By integrating DEM data, soil moisture maps, and vehicle kinematic parameters into a GA, the study ensures that the paths adhere to safety constraints such as avoiding wet areas and maintaining permissible roll and pitch angles. This approach not only reduces the length of the path, but also safeguards the integrity and operational safety of the vehicle in challenging environments, avoiding expensive mistakes and the need for manual intervention.

The results of this study were obtained using a single combination of parameters to facilitate comparison between the models. A sensitivity analysis of the parameters, which could potentially improve the model's performance, was outside the scope of the paper due to the extensive work needed to explore the many possible parameter variations. Additionally, the focus of this work is on presenting the novelty of this GCPP methodology, rather than finding the optimal solution for the sites in this study.

In the current setup, calculating 100 nodes takes 43 minutes. The main reason for the long calculation time is the complexity of the problem, but also a limitation resulting in single-threaded calculations. Despite having a 20-thread processor, only one permutation can be processed at a time due to reliance on a single thread. In theory, enabling multi-threading could speed up the calculation by allowing the processor to handle 20 permutations simultaneously. However, in practice, multi-threading took longer than single-threading. The overhead of distributing permutations across multiple threads and aggregating the results proved more time-consuming than performing the calculation sequentially on a single thread. If this could be solved, it could speed up the calculations. On the other hand, this will not impact the results of this study, except for the calculation time.

Despite the single-threaded limitation, the calculation can be completed well in advance of the vehicle driving on the site,

allowing it to take time. The energy and time invested in solving the problem can be justified by the reduction of driving distance during vehicle operation.

The study evaluated two primary grid discretization techniques, a square grid and an equilateral triangular grid. Statistical analysis revealed that the square-aligned pattern produced shorter paths for site 3. For sites 1 and 2, the results varied based on the specific node configuration. These findings suggest that the effectiveness of a node configuration is site-specific, indicating that no single node configuration is suitable across all sites. Thus, more research is needed to fully evaluate the best performing grid alignment method.

As shown in Table 1, the triangular grid pattern consistently converged to the same path length, while the square grid pattern tended to converge to different local minima. We hypothesize that the crossover and mutation mechanisms used in this study are better suited to the triangular grid structure because its more equidistant neighboring nodes promote more consistent convergence. For site 1, Table 1 highlights that the square grid results in the shortest path. However, a large variation is apparent since this same grid configuration also produces one of the longest paths. A possible explanation is that site 1 is a real-world test site with a more complex DEM compared to the synthetic sites, resulting in a greater number of local minima. In contrast, when using a triangular grid, Site 1 converges only one solution, suggesting that the square grid is more prone to getting trapped in local minima. For the end user, this implies that a triangular grid can be used to achieve consistent and reasonably good results with a single run. In contrast, a square grid demonstrated variability in performance, which means results could either be better or worse compared to those from the triangular grid. If the end user prioritizes obtaining a short path over calculation time, the square grid can be utilized, allowing the selection of the shortest path from multiple runs. However, if calculation time is the primary concern, the triangular grid is preferable as it only requires one calculation to produce consistent results.

Although site 3 has a similarity between the square aligned node pattern and the square straight, a difference with statistical significance between the methods was shown. Since the pattern was rotated 90° around the centroid of the site, a slight difference between the grids occurred likely caused by node positioning within the critical gradient area.

A border effect was observed in certain cases, particularly when nodes were positioned near the border and the terrain sloped toward it. This situation caused the GCPP to take more time to generate an acceptable path. The issue arises because nodes near the border, face limited path options due to boundary restrictions, compounded by pitch and roll constraints. These combined limitations often resulted in paths that exceeded the set constraints.

Conclusions

The objective for this study was to develop a method for generating short, efficient routes for ground-based forest operations while considering environmental factors such as soil moisture and vehicle parameters such as turning radius, working width, roll, and pitch angles. This was accomplished by formulating a fitness function that calculated the Dubins path distance while ensuring vehicle safety by penalizing solutions that exceeded vehicle constraints, and a GA approach was proposed to optimize node sequencing for the TSP. Through evaluation of different grid discretization techniques, including triangular and square grids, the study demonstrated that no specific node pattern reduced the path lengths of all sites, suggesting that the node patterns are site specific. The square grid approach was able to find shorter paths than the triangular, but only seldomly. While the triangular grid converged to the same fitness value every time, the square grid had a variation between runs.

The results show that the GCPP generates a path that respects the vehicle constraints, while iteratively reducing the path distance. The time and energy spent on computations can be justified by the reduction in driving distance during deployment.

Future work

Future research directions suggest integrating energy considerations into the fitness function for reduced fuel consumption (Dogru and Marques 2015b; Wu et al. 2019; Qiu et al. 2024) and conducting physical validation tests to assess the practical applicability of the proposed method and map data. Additionally, sensitivity analyses on grid size to turning radius factors could provide further insights into route planning optimizations. Integrating coverage into the fitness function would also be interesting since this article only implies coverage from the uniform spacing of nodes within the grid. By linearizing the problem, larger problems with more nodes can be solved. This can be done by dividing larger sites into different sections, such as clustering the nodes, which reduces the calculation time (Romanuke 2024).

The parameters used in GA were empirically derived to suit various grid sizes and sites, specifically tailored to the Research Vehicle Platform. While these parameters were mainly chosen to demonstrate the methodology, it would be valuable to explore

combinations that are tailored to different grid patterns, as well as more general combinations that could be applied to a wider range of vehicles. Since the parameters in this study primarily served as a proof of concept, future research is needed to identify other parameter configurations.

To address the border effect where the GCPP encounters difficulty in generating acceptable paths near borders with sloping terrain, we propose that users are granted the flexibility to adjust node positions manually during post-processing stages. This should allow users to strategically relocate nodes, thereby overcoming problematic areas and improving the overall quality of generated paths. Alternatively, an automatic function can be developed to iteratively evaluate relocation of problematic nodes until the fitness function is penalty-free.

During Dubins path calculation, only the traversability of the vehicle's centerpoint is evaluated, which can induce errors if the width of the vehicle exceeds the resolution of the digital elevation model. This can be derived from Figure 4 and can result in boundary effects where the edge of the vehicle follows an unacceptable trail, despite being considered acceptable by the route planner.

To implement this coverage path planner in forest operations such as planting, it is beneficial to consider factors such as reloading plants and refueling. This involves calculating multiple paths if the plant capacity is insufficient to meet the site demands. Consequently, solving a vehicle routing problem becomes necessary instead of the traveling salesman problem. By solving the vehicle routing problem, it also opens possibilities for deploying multiple vehicles on the same site simultaneously.

Acknowledgements

This research was partly conducted within Trees For Me, a center of excellence supported by the Swedish Energy Agency and almost 50 stakeholders with grant number [P2021-90272]. In addition, this work was supported by AutoPlant, which was funded by the Swedish Innovation Agency, VINNOVA with grant number [2023-02747].

Disclosure statement

No potential conflict of interest was reported by the author(s).

ORCID

Erik Arvidsson  <http://orcid.org/0000-0001-7679-0203>
 Magnus Karlberg  <http://orcid.org/0000-0002-2342-1647>
 Håkan Lideskog  <http://orcid.org/0000-0002-9862-828X>
 Torbjörn Lindbäck  <http://orcid.org/0000-0002-6209-9355>

Author contributions

E.A. was the main contributor to the project, including data collection, data processing, tool creation, analysis, and paper writing. M.K., H.L., and T.L. provided essential supervision and support throughout the process, providing guidance, reviewing the work, and approving the final article.

References

Bostelmann-Arp L, Steup C, Mostaghim S. 2023. Multi-objective seed curve optimization for coverage path planning in precision farming.

- Annual Conference on Genetic and Evolutionary Computation. doi: [10.1145/3583131.3590490](https://doi.org/10.1145/3583131.3590490).
- Cabreira TM, Brisolara LB, Ferreira PR Jr. 2019. Survey on coverage path planning with unmanned aerial vehicles. *Drones*. 3(1):4. doi: [10.3390/drones3010004](https://doi.org/10.3390/drones3010004).
- Choset H. 2000. Coverage of known spaces: the boustrophedon cellular decomposition. *Auton Robots*. 9(3):247–253. doi: [10.1023/A:1008958800904](https://doi.org/10.1023/A:1008958800904).
- Dogru S, Marques L. 2015a. Energy efficient coverage path planning for autonomous mobile robots on 3d terrain. 2015 IEEE International Conference on Autonomous Robot Systems and Competitions. doi: [10.1109/ICARSC.2015.23](https://doi.org/10.1109/ICARSC.2015.23).
- Dogru S, Marques L. 2015b. Towards fully autonomous energy efficient coverage path planning for autonomous mobile robots on 3d terrain. 2015 European Conference on Mobile Robots (ECMR). doi: [10.1109/ECMR.2015.7324206](https://doi.org/10.1109/ECMR.2015.7324206).
- Dubins LE. 1957. On curves of minimal length with a constraint on average curvature, and with prescribed initial and terminal positions and tangents. *Am J Math*. 79(3):497–516. doi: [10.2307/2372560](https://doi.org/10.2307/2372560).
- Hameed I, Cour-Harbo AL, Osen O. 2016. Side-to-side 3d coverage path planning approach for agricultural robots to minimize skip/overlap areas between swaths. *Robot Auton Syst*. 76:36–45. doi: [10.1016/j.ROBOT.2015.11.009](https://doi.org/10.1016/j.ROBOT.2015.11.009).
- Hameed IA. 2014. Intelligent coverage path planning for agricultural robots and autonomous machines on three-dimensional terrain. *J Intell Robot Syst*. 74(3–4):965–983. doi: [10.1007/S10846-013-9834-6](https://doi.org/10.1007/S10846-013-9834-6).
- Han Y, Shao M, Wu Y, Zhang X. 2022. An improved complete coverage path planning method for intelligent agricultural machinery based on backtracking method. *Information*. 13(7):313. doi: [10.3390/info13070313](https://doi.org/10.3390/info13070313).
- Hansson LJ, Sten G, Rossander M, Lideskog H, Manner J, van Westendorp R, Li S, Eriksson A, Wallner A, Rönnqvist M, et al. 2024. Autoplant—autonomous site preparation and tree planting for a sustainable bioeconomy. *Forests*. 15(2):263. doi: [10.3390/f15020263](https://doi.org/10.3390/f15020263).
- Hera PL, Mendoza-Trejo O, Lindroos O, Lideskog H, Lindbäck T, Latif S, Li S, Karlberg M. 2024. Exploring the feasibility of autonomous forestry operations: results from the first experimental unmanned machine. *J Field Robot*. doi: [10.1002/ROB.22300](https://doi.org/10.1002/ROB.22300).
- Jin J. 2009. Optimal field coverage path planning on 2d and 3d surfaces. doi: [10.31274/ETD-180810-3122](https://doi.org/10.31274/ETD-180810-3122).
- Jin J, Tang L. 2011. Coverage path planning on three-dimensional terrain for arable farming. *J Field Robot*. 28(3):424–440. doi: [10.1002/ROB.20388](https://doi.org/10.1002/ROB.20388).
- Jourgholami M, Hansson LJ, Högbom L, Jourgholami M, Laschi A. 2022. Strategies to mitigate the effects of soil physical disturbances caused by forest machinery: a comprehensive review. doi: [10.1007/S40725-021-00155-6](https://doi.org/10.1007/S40725-021-00155-6).
- Lantmäteriet. 2024. Quality description - national height model (kvalitetsbeskrivning nationell markhöjdmodell). Swedish. [accessed 2024 Feb 8]. https://www.lantmateriet.se/globalassets/geodata/geodataproducter/hojddata/kvalitetsbeskrivning_mhm.pdf.
- Lidberg W. 2019. Digital wet areas mapping [Ph.D. thesis]. Swedish University of Agricultural Sciences. https://pub.epsilon.slu.se/15989/17/lidberg_w_190312.pdf.
- Lideskog H, Karlberg M, Bergsten U. 2015. Development of a research vehicle platform to improve productivity and value-extraction in forestry. *Procedia CIRP*. 38:68–73. doi: [10.1016/j.procir.2015.07.014](https://doi.org/10.1016/j.procir.2015.07.014).
- Lund E. 2016. Annual working units (awu) in forestry labour by region and type of operator. year (3-years average) 1976–2016. [accessed 2024 Apr 30]. <https://pxweb.skogsstyrelsen.se:443/sq/1f11305d-7195-4225-bb82-bb097b4ddf90>.
- Man K, Tang K, Kwong S. 1996. Genetic algorithms: concepts and applications [in engineering design]. *IEEE Trans Ind Electron*. 43(5):519–534. doi: [10.1109/41.538609](https://doi.org/10.1109/41.538609).
- Mann HB, Whitney DR. 1947. On a test of whether one of two random variables is stochastically larger than the other. *Ann Math Statist*. 18(1):50–60. doi: [10.1214/aoms/1177730491](https://doi.org/10.1214/aoms/1177730491).
- Nilsson RS, Zhou K. 2020. Method and bench-marking framework for coverage path planning in arable farming. *Biosyst Eng*. 198:248–265. doi: [10.1016/j.biosystemseng.2020.08.007](https://doi.org/10.1016/j.biosystemseng.2020.08.007).
- Qiu W, Zhou D, Hui W, Kwabena AR, Xing Y, Qian Y, Quan L, Pu H, Xie Y. 2024. Terrain-shape-adaptive coverage path planning with traversability analysis. *J Intell Robot Syst*. 110(1). doi: [10.1007/S10846-024-02073-8](https://doi.org/10.1007/S10846-024-02073-8).
- Ringdahl O. 2011. Automation in forestry: development of unmanned forwarders [Ph.D. thesis]. Umeå University, Department of Computing Science.
- Romanuke VV. 2024. Deep clustering of the traveling salesman problem to parallelize its solution. *Comput Oper Res*. 165:106548. doi: [10.1016/j.cor.2024.106548](https://doi.org/10.1016/j.cor.2024.106548).
- Savilaakso S, Johansson A, Häkkilä M, Uusitalo A, Sandgren T, Mönkkönen M, Puttonen P. 2021. What are the effects of even-aged and uneven-aged forest management on boreal forest biodiversity in fennoscandia and European Russia? a systematic review. *Environ Evid*. 10(1):1. doi: [10.1186/s13750-020-00215-7](https://doi.org/10.1186/s13750-020-00215-7).
- Sikström U, Hjelm K, Hanssen KH, Saksa T, Wallertz K. 2020. Influence of mechanical site preparation on regeneration success of planted conifers in clearcuts in fennoscandia – a review. *Silva Fenn*. 54(2). doi: [10.14214/sf.10172](https://doi.org/10.14214/sf.10172).
- Swedish Forest Agency. 2022a. Gross and net felled volume (million m³) by assortment of stemwood. year 1942–2022. [accessed 2024 Apr 30]. <https://pxweb.skogsstyrelsen.se:443/sq/5dc11401-3ae7-40fb-ad2d-348dd55dd44f>.
- Swedish Forest Agency. 2022b. 09. mean, median, and 95th percentile in (ha) for annual final harvests within reports larger than or equal to 0.5 hectares by region, ownership category, variable, and year. Swedish. [accessed 2024 Feb 20]. <https://pxweb.skogsstyrelsen.se:443/sq/fddaf781-d7f0-4938-9ed9-b1dd4be0394>.
- Swedish Forest Agency. 2022c. Skogsårslagsstiftningen 2022 (Swedish forestry act 2022). Swedish. [accessed 2024 May 1]. <https://www.skogsstyrelsen.se/globalassets/lag-och-tillsyn/skogsvardslagen/skogsvardslag-stiftningen-gallande-fran-1-september-2022.pdf>.
- Nordfjell T, Rolf Björheden MT, Wästerlund I. 2010. Changes in technical performance, mechanical availability and prices of machines used in forest operations in Sweden from 1985 to 2010. *Scand J For Res*. 25(4):382–389. doi: [10.1080/02827581.2010.498385](https://doi.org/10.1080/02827581.2010.498385).
- Nordfjell T, Emil Öhman OL. 2019. The technical development of forwarders in Sweden between 1962 and 2012 and of sales between 1975 and 2017. *Int J For Eng*. 30(1):1–13. doi: [10.1080/14942119.2019.1591074](https://doi.org/10.1080/14942119.2019.1591074).
- Wu C, Dai C, Gong X, Liu YJ, Wang J, Gu X, Wang CCL. 2019. Energy-efficient coverage path planning for general terrain surfaces. *IEEE Robotics and Automation Letters*. doi: [10.1109/LRA.2019.2899920](https://doi.org/10.1109/LRA.2019.2899920).
- Yasutomi F, Yamada M, Tsukamoto K. 1988. Cleaning robot control. Proceedings. 1988 IEEE International Conference on Robotics and Automation vol. 3. p. 1839–1841. doi: [10.1109/ROBOT.1988.12333](https://doi.org/10.1109/ROBOT.1988.12333).
- Örlander G, Gemmel P, Hunt J. 1990. Site preparation: a Swedish overview. FRDA Report (Victoria, B.C.) 105.